

Constraints of Dark Energy at High Redshift

Qiping Su^{a,1}, Rong-Gen Cai²

¹Department of Physics, Hangzhou Normal University, Hangzhou, 310036, China

²State Key Laboratory of Theoretical Physics, Institute of Theoretical Physics, Chinese Academy of Sciences, P.O. Box 2735, Beijing 100190, China

Received: date / Accepted: date

Abstract Constrains of dark energy (DE) at high redshift from current and mock future observational data are obtained. It is found that present data give poor constraints of DE even beyond redshift $z=0.4$, and mock future 2298 type Ia supernove data only give a little improvement of the constraints. We analyze in detail why constraints of DE decrease rapidly with the increasing of redshift. Then we try to improve the constraints of DE at high redshift. It is shown that the most efficient way is to improve the error of observations.

1 Introduction

The current expansion of the universe is found to be in accelerating [1,2] and it is believed that the dark energy (DE), whose equation of state $w_{de} = p_{de}/\rho_{de}$ is less than $-1/3$, plays the role to drive the accelerated expansion of the universe. Plenties of DE models have been proposed [3,4,5,6,7,8,9] but the origin of DE is still unknown. We have only known a little about DE from observations.

Several parametrization methods of w_{de} have been proposed to fit with observations to get constraints of w_{de} . Usually in parametrization models w_{de} is assumed to be a simple function of redshift z , e.g., the CPL parametrization [10,11]: $w_{de}(z) = w_0 + w_a z/(1+z)$, and the parametrization of redshift expansion [12,13]: $w_{de}(z) = w_0 + w_z z$. It has been found that w_{de} is very close to -1 and is varying very slowly (if it is dynamical). But these fitting results depend on the parametrization forms of $w_{de}(z)$ used. Moreover, one parametrization form of $w_{de}(z)$ could only approximate the real w_{de} well in a very limited region of redshift. So fitting results from a single model should not be used to analyzing

behaviors of DE at both low and high redshift. There are also “model-independent” methods[14,15,16,17], in which the redshift of data is usually divided into several bins and in each redshift bin w_{de} is assumed to be a simple function of z . All “model-independent” methods show that constraints of w_{de} at higher redshift are much weaker than that at low redshift [18,19,20,21,22,23]. It is important and necessary to get good constraints of w_{de} at high redshift to reveal the nature of DE, such as the dynamical behaviors of DE.

In this paper, we’d like to analyze constraints of w_{de} at high redshift. Since present constraints of DE are from observational data, we will mainly analyze effects of observational data on constraining DE at high redshift. We will start with type Ia supernovae (SnIa) data. Almost all present data for DE are related to the comoving distance and the most data of this distance type are from SnIa. Commonly used DE data other than the distance type are CMB data and Hubble parameter data only. And main information in CMB data can be extracted to distance priors (such as the shift parameter R date): there is only a little difference between constraints of DE from full CMB data and from the distance priors[24]. The distance priors are related to distances, i.e., one can convert the CMB data to data of distance type. So our analyses will be mainly based on the distance type of data, and study why distance type of data give poor constraints of DE at high redshift.

The paper is organized as follows. In section II, constraints of w_{de} at low redshift and high redshift from present and mock future data are obtained. In section III, we analyze the properties of w_{de} at high redshift in detail and try to find out reasons of the poor constraints. In section IV, we try to improve constraints of w_{de} at high redshift by adding number of data points,

^ae-mail: sqp@hznu.edu.cn

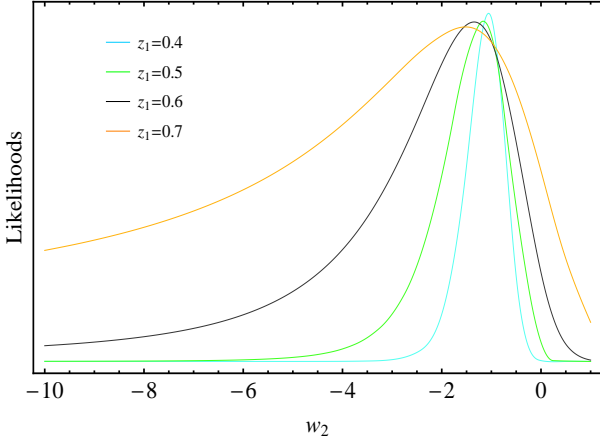


Fig. 1 The likelihoods of w_2 from present data, with divided position $z_1=0.4, 0.5, 0.6, 0.7$, respectively.

decreasing error of observational data and adding other type of data (i.e., Hubble parameter data).

2 Constraints from distance type of data

At present, almost all observational data for DE are the distance type, such as data of SnIa, BAO parameter A and CMB shift parameter R , which are related to a comoving distance: $r_c = \int dt/a = \int dz/H(z)$. At first, we'd like to estimate the effect of SnIa data (since it gives the most data points for DE) on constraints of DE, especially constraints at high redshift. Since a single SnIa data set has poor constraints on DE, the BAO parameter A will also be adopted to alleviate the degeneracy between equation of state (w_{de}) and dimensionless density energy (Ω_{de}) of DE.

We will use the UBE method to get constraints of w_{de} from present and future mock data. We divide the redshift of data into two bins and set

$$w_{de}(z) = \begin{cases} w_1, & 0 \leq z \leq z_1 \\ w_2, & z_1 < z \end{cases}, \quad (1)$$

where w_1 and w_2 are just constants and z_1 is the divided position of low and high redshift. In the numerical calculations we will set the prior $w_2 > -20$, or w_2 will run to large minus value in MCMC procedure and the lower error of w_2 will be extremely large. This will be discussed in detail in the next section. For each data set the figure of merit (FoM) [25,26] is also calculated, which is defined as:

$$\text{FoM} = [\det C(w_1, w_2)]^{-1/2}, \quad (2)$$

where $C(w_1, w_2)$ is the covariance matrix of w_1 and w_2 after marginalizing out all other parameters. In general, FoM is used to estimate the goodness of the data in constraining w_{de} .

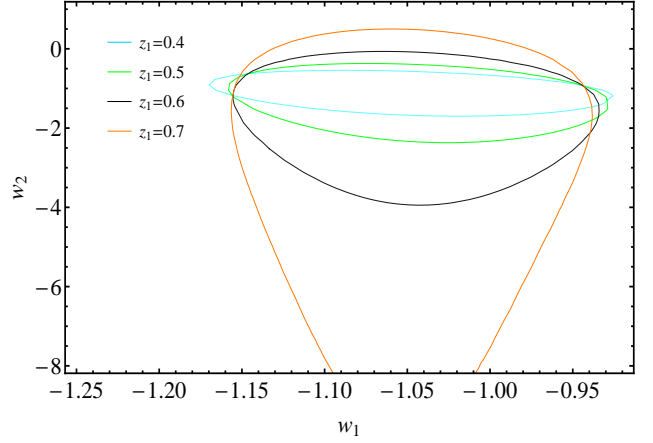


Fig. 2 68% C.L. contour plot in $w_1 \sim w_2$ plane from present data, with divided position $z_1=0.4, 0.5, 0.6, 0.7$, respectively.

Our calculations show that the correlation between w_1 and w_2 is very small, i.e., the errors of w_1 and w_2 obtained can be treated as independent with each other. So errors of w_2 (w_1) just represents constraints of w_{de} at high (low) redshift.

2.1 Constraints from present data set

Here we get constraints of w_{de} from Union2.1 SnIa data [27] and BAO Parameter A data from [28]. To estimate constraints of w_{de} at different high redshift bins, the divided position z_1 will be set as 0.4, 0.5, 0.6 and 0.7, respectively. The best-fitted parameters and their 68.3%, 95.4% confidence level (C.L.) errors are obtained by using the Markov chain Monte Carlo (MCMC) method, which are shown in Table 1. We have following conclusions:

1. w_{de} at high redshift ($z > 0.4$) are highly unconstrained by present data, especially compared with w_{de} at low redshift. With $z_1 = 0.4$, the average 95.4% C.L. error for w_2 (noted as $2\bar{\sigma}(w_2)$) is

$$2\bar{\sigma}(w_2) = (0.67 + 1.05)/2 = 0.86$$

and $2\bar{\sigma}(w_1)$ is only about 0.15, as shown in Table 1.

z_1	w_1	w_2	FoM
0.4	$-1.04^{+0.03+0.14}_{-0.09-0.17}$	$-1.04^{+0.36+0.67}_{-0.43-1.05}$	28.47
0.5	$-1.04^{+0.07+0.14}_{-0.08-0.17}$	$-1.19^{+0.68+1.15}_{-0.92-2.43}$	12.68
0.6	$-1.04^{+0.06+0.13}_{-0.08-0.18}$	$-1.33^{+1.30+2.13}_{-2.87-18.52}$	3.52
0.7	$-1.04^{+0.06+0.12}_{-0.09-0.17}$	$-1.50^{+2.14+2.44}_{-14.84-18.47}$	2.36

Table 1 The best-fitted values and their 68.3% and 95.4% C.L. errors of w_1 and w_2 from present observational data, the divided positions are $z_1 = 0.4, 0.5, 0.6, 0.7$, respectively.

2. Errors of w_{de} at high redshift (i.e., errors of w_2) increase rapidly with the divided point z_1 , especially the lower errors of w_2 . As shown in Fig. 1, z_1 is larger, the likelihood of w_2 decreases more slowly with the decreasing of w_2 . We will analyze this phenomenon in detail in the next section.

3. Effect of the divided position z_1 on errors of w_{de} at low redshift (i.e., w_1) is very weak. As shown in Table. 1, with the increasing of z_1 variations of errors of w_1 are negligible. It implies that present data set at low redshift ($z < 0.4$) is sufficient and constraints on w_{de} in this region is strong.

4. Here, values of FoM can be used to estimate goodness of constraints of w_{de} at high redshift. FoM from Eq.(2) is proportional to the inverse area of the 1σ error ellipse in the $w_1 \sim w_2$ plane. As shown from the contour plots in Fig. 2 and errors of w_1 in Table 1, the decreasing of FoM (with respect to the increasing of z_1) is due to the increasing of errors of w_2 . So value of FoM is larger, errors of w_2 are smaller, and vice versa. Indeed, FoM increases rapidly with the decreasing of z_1 , as shown in Table 1 and Fig. 5.

2.2 Constraints from future data

To estimate the constraints of w_{de} at high redshift from future data, we fit the 2-binned UBE model with 2298 simulated SNIa data (denoted as elementary data set in this paper), which contain 1998 SNIa data with redshift $0.1 < z < 1.7$ from a SNAP-like JDEM survey and 300 SNIa data with $z < 0.1$ from the NSNF [30,31]. To alleviate the degeneracy between Ω_{m0} and w_{de} [32], the date of BAO Distance Parameter A [28] will also be included. To simulate the mock SNIa data, we assume the fiducial model as $w_{de}(z) = -1$. The error of the distance modulus (δ) for each supernova is set as 0.13 [17]. To estimate the effect of the divided position z_1 , we have set z_1 as 0.4, 0.6, 0.8 and 1.0, respectively.

As shown in Table 2, with much more data points, the errors of w_{de} from future data are smaller than that from the present data. E.g., here $2\bar{\sigma}(w_2) = 0.43$ for $z > 0.4$, which is just a half of that from the present

z_1	w_1	w_2	FoM
0.4	$-0.96^{+0.03+0.07}_{-0.04-0.09}$	$-1.12^{+0.17+0.30}_{-0.24-0.55}$	119.65
0.6	$-0.97^{+0.03+0.08}_{-0.06-0.12}$	$-1.14^{+0.27+0.45}_{-0.42-1.31}$	33.23
0.8	$-0.96^{+0.04+0.08}_{-0.07-0.15}$	$-1.11^{+0.43+0.73}_{-0.69-4.03}$	11.68
1.0	$-0.95^{+0.02+0.06}_{-0.08-0.15}$	$-1.11^{+0.89+1.28}_{-1.88-18.73}$	5.89

Table 2 The best-fitted values and their 68.3% and 95.4% C.L. errors of w_1 and w_2 from mock future data, the divided positions are $z_1 = 0.4, 0.6, 0.8, 1.0$, respectively.

data (i.e., 0.86). Errors of w_{de} at high redshift (i.e., w_2) also increase rapidly with z_1 , e.g., here $2\bar{\sigma}(w_2)$ for $z > 0.6$ is 0.88. It also shows that constraints of w_{de} beyond $z = 1$ are extremely weak. On the other hand, constraints of w_{de} at low redshift (i.e., constraints of w_1) are also improved, but not as much as that of w_2 .

In all, present data gives poor constraints of w_{de} at high redshift (e.g., $z > 0.4$), and the mock future 2298 SNIa data do not give sufficient improvement on constraints of w_{de} at high redshift.

3 Analyzing constraints

Now we try to answer two questions:

3.1 Why data of distance type give poor constraints on w_{de} at high redshift?

Reasons are:

1. Data points in a redshift bin will constrain w_{de} in this bin and in lower redshift bins, but can not constrain w_{de} in higher redshift bins, e.g., w_{de} in the lowest redshift bin can be constrained by all data points. Moreover, the redshift is larger the corresponding distance is farther, and it will be harder to measure the distance. And the farther a supernova is, the harder it can be detected. While the most data points for DE are from SNIa. In all, there are much less efficient data points in higher redshift bins.

2. In higher redshift, the effect of dark energy on the luminosity distance

$$D_l(z) = (1+z) \int_0^z dz' / H(z') \quad (3)$$

is much less. Here $H^2(z') \sim \rho_{de}(z') + \rho_{dm}(z')$. With respect to the increase of redshift z , energy density of DE (ρ_{de}) evolves very slowly, while energy density of DM (ρ_{dm}) increases very rapidly since $\rho_{dm} \sim (1+z)^3$. In higher redshift bin, ρ_{de} is much less than ρ_{dm} . So constraints of DE at high redshift from distance type of data will be weaker.

3.2 Why lower errors of w_{de} at high redshift bins are extremely large

This can be shown by simple calculations as follows. In a flat FRW universe the Friedmann equation reads:

$$H^2(x) = \frac{1}{3}[\rho_{m0}(1+x)^3 + \rho_{de}(x)], \quad (4)$$

where $\rho_{de}(x) = \rho_{de0} e^{3 \int_0^x \frac{1+w_{de}(y)}{1+y} dy}$.

$$\delta D_l(z) = \begin{cases} 0, & 0 \leq z \leq z_i \\ -\frac{3}{2}(1+z) \int_{z_i}^z \frac{\delta w_i}{H(x)} \Omega_{de} \ln\left(\frac{1+x}{1+z_i}\right) dx, & z_i < z \leq z_{i+1} \\ -\frac{3}{2}(1+z) \left[\int_{z_i}^{z_{i+1}} \frac{\delta w_i}{H(x)} \Omega_{de} \ln\left(\frac{1+x}{1+z_i}\right) dx + \int_{z_{i+1}}^z \frac{\delta w_i}{H(x)} \Omega_{de} \ln\left(\frac{1+x_{i+1}}{1+z_i}\right) dx \right], & z_{i+1} < z \end{cases} \quad (5)$$

The redshift is divided into n bins and in each bin w_{de} is set as a constant. Supposing there is a tiny variation of w_{de} in the i^{th} bin (δw_i) and no variations of w_{de} in all other bins, from Eq.(3) and (4) one gets

$$\delta H^2(x) = \begin{cases} 0, & 0 \leq x \leq z_i \\ \rho_{de} \ln\left(\frac{1+x}{1+z_i}\right) \delta w_i, & z_i < x \leq z_{i+1} \\ \rho_{de} \ln\left(\frac{1+z_{i+1}}{1+z_i}\right) \delta w_i, & z_{i+1} < x \end{cases} \quad (6)$$

and Eq.(5) for $\delta D_l(z)$, where $\Omega_{de} = \rho_{de}/(\rho_{de} + \rho_{dm})$.

One can see that δw_i always appears together with Ω_{de} in Eq.(5). At higher redshift (i.e., larger i), with the same δw_i Ω_{de} is much smaller and $\delta D_l(z)$ is also smaller. It indicates that the redshift is higher, to lead to the same variation of D_l the variation of w_i must be larger, i.e., $D_l(z)$ is less sensitive to w_i at higher redshift. In all, constraints on w_{de} from the luminosity distance are weaker in higher redshift bins.

As shown in Eq.(5), δD_l in the i^{th} bin is related to an integration, which is mainly determined by Ω_{de} and the width of this redshift bin. The width of a redshift bin is larger, the integration will be larger and so will be δD_l . In higher redshift bins Ω_{de} is smaller since

$$\Omega_{de}(z_i < z < z_{i+1}) \sim (1+z)^{3w_i}, \quad (7)$$

so δD_l will be smaller. Note that Ω_{de} is also dependent on w_i

Now let's answer the question. In a high redshift bin if w_i is much smaller than -1 , Ω_{de} in this bin will be so small that δD_l keeps small even the bin is wide and δw_i is large, i.e. with different small values of w_i one gets almost the same D_l . In this case, the likelihood of w_i will be very flat for $w_i \ll -1$ as shown in Fig. 1. Thus the lower errors of w_i at high redshift bins are always extremely large. In general, the constraint of w_{de} in the last redshift bin is the weakest.

multiple	w_1	w_2	FoM
$\times 2$	$-0.96^{+0.03+0.06}_{-0.08-0.13}$	$-1.33^{+0.82+1.13}_{-1.95-18.64}$	6.64
$\times 3$	$-1.00^{+0.02+0.06}_{-0.05-0.11}$	$-1.01^{+0.54+0.93}_{-0.86-3.48}$	15.41
$\times 4$	$-1.00^{+0.03+0.06}_{-0.04-0.08}$	$-1.20^{+0.49+0.89}_{-0.72-2.49}$	22.03
$\times 5$	$-0.99^{+0.02+0.05}_{-0.04-0.06}$	$-1.00^{+0.37+0.65}_{-0.47-1.27}$	92.48

Table 3 The best-fitted values and their 68.3% and 95.4% C.L. errors of w_1 and w_2 from simulated SnIa data. The numbers of SnIa data are 2, 3, 4, and 5 times of the 2298 elementary data, respectively. The divided position z_1 is set to 1.0.

4 Improving constraints

According to previous results and analyses, we try to improve the constraints of w_{de} at high redshift. Three methods will be implemented and their efficient will be compared.

4.1 Adding the number of SnIa data

In the section 2.2 it is shown that ~ 2300 mock future SnIa data still give poor constraints of w_{de} beyond $z \sim 0.6$. Here we try to use more mock SnIa data, with 2, 3, 4 and 5 times of the 2298 elementary data. The proportional distribution of redshift in these multiple date sets is the same as the elementary date set. The divided position z_1 of the two bins is now set to 1.0. The results are shown in Table 3. It shows that FoM increases with the increasing of number of date points, but the increase is not very efficient. With 5 times number of the elementary SnIa date set (about 11500 supernovae), constraints of w_{de} beyond $z = 1$ are still weak: $2\bar{\sigma}(w_2) = 0.96$.

4.2 Improving accuracy of the data

Increasing the number of SnIa data seems not efficient enough in improving constraints of w_{de} at high redshift. It is expected that with the increase of number of data the statistical errors of the data will be decreased. Moreover, the systematic errors of the data will be improved by future observations [33]. To estimate effects of the error δ of distance modulus of supernovae, here we set $\delta = 0.13, 0.1, 0.05, 0.02$, respectively. The num-

δ	w_1	w_2	FoM
0.13	$-1.00^{+0.02+0.06}_{-0.05-0.11}$	$-1.01^{+0.54+0.93}_{-0.86-3.48}$	15.41
0.10	$-1.00^{+0.01+0.05}_{-0.04-0.07}$	$-1.01^{+0.41+0.72}_{-0.55-1.52}$	30.57
0.05	$-1.00^{+0.01+0.03}_{-0.01-0.04}$	$-1.01^{+0.22+0.39}_{-0.24-0.55}$	386.48
0.02	$-1.00^{+0.00+0.00}_{-0.00-0.01}$	$-1.00^{+0.08+0.16}_{-0.09-0.19}$	2478.16

Table 4 The best-fitted values and their 68.3% and 95.4% C.L. errors of w_1 and w_2 with errors in distance modulus $\delta = 0.13, 0.10, 0.05, 0.02$, respectively. The number of SnIa used is 3 times of 2298 elementary SnIa data. The divided positions z_1 is set to 1.0.

z_1	w_1	w_2	FoM
0.4	$-1.03^{+0.08+0.15}_{-0.07-0.16}$	$-0.86^{+0.20+0.37}_{-0.25-0.54}$	72.22
0.5	$-1.03^{+0.08+0.15}_{-0.05-0.14}$	$-0.82^{+0.25+0.45}_{-0.35-0.84}$	50.45
0.6	$-1.03^{+0.07+0.14}_{-0.05-0.14}$	$-0.74^{+0.30+0.48}_{-0.50-1.39}$	35.56
0.7	$-1.04^{+0.10+0.15}_{-0.03-0.11}$	$-0.67^{+0.34+0.53}_{-0.76-2.78}$	13.13

Table 5 The best-fitted values and their 68.3% and 95.4% C.L. errors of w_1 and w_2 from data of SN+A+R, the divided positions are $z_1 = 0.4, 0.5, 0.6, 0.7$, respectively.

ber of the SnIa data used here will be 3 times of the elementary data and $z_1 = 1.0$ is set.

The results in Table 4 show that FoM increases very rapidly with the decrease of δ . With $\delta = 0.02$, $2\bar{\sigma}(w_2) = 0.18$ for $z > 1.0$, which is a good constraint of w_{de} at high redshift.

Of course, the errors of other distance type of observations are also improved continually. For example, the 1σ error of CMB shift parameter R from WMAP9 is 0.016[34], which decreased to 0.009 from Planck[35]. This parameter is defined as:

$$R = \sqrt{\Omega_{m0}} \int_0^{z_s} \frac{dz}{E(z)}, \quad E = H/H_0$$

which is related to the distance of decoupling epoch ($z_s \sim 1091$ is the redshift of decoupling).

Now We combine shift parameter R from WMAP9 with Union2.1 and BAO data to get constraints of w_{de} . Main results are shown in Table 5. In Fig. 3, FoM for this date set are plotted to compare with other date sets. With the addition of shift parameter R, $2\bar{\sigma}(w_2) = 0.28$ for $z_1 = 0.4$, without this parameter $2\bar{\sigma}(w_2) = 0.86$ for $z_1 = 0.4$.

The addition of a single date point R gives a big improvement of FoM and constraints of w_{de} at high redshift, main reasons are:

- 1) The error of R date (0.016) is very small, compared with the present errors of SnIa. As shown in previous results, the error of date is smaller, the constraints of w_{de} will be better. Moreover, the corresponding redshift for the parameter R is $z \sim 1091$, it gives good constraints of w_{de} in all redshift bins.
- 2) To involve the date of parameter R, the second redshift bin should be $(z_1, 1091)$. As analyzed in section 3.2, the bigger a redshift bin is, the effect of w_{de} on D_I will be bigger. So the constraint of w_2 from parameter R is good.
- 3) The shift parameter R date can further alleviate the degeneracy between w_{de} and Ω_{de} .

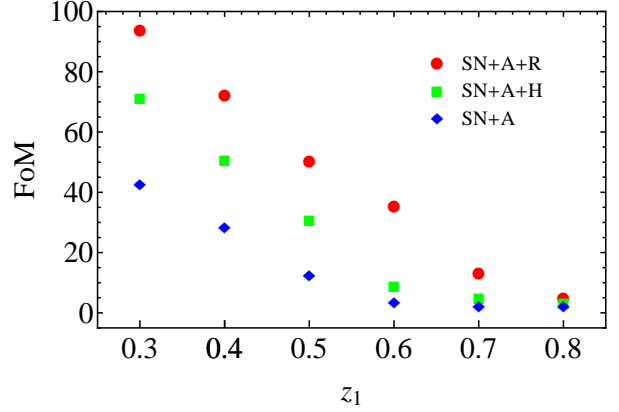


Fig. 3 Values of FoM from SN+A+R (dots), SN+A+H (squares) and SN+A (diamonds), where SN is for Union2.1 SnIa date, A is for the BAO date, R is for the shift parameter date and H is for 22 Hubble parameter data. The abscissa is for the divided position z_1 .

4.3 Combined with other type of data

There is few type of date other than distance type, the typical one is the Hubble parameter data which constrain w_{de} directly: there is no integration between the Hubble parameter and w_{de} .

Here we combine 22 Hubble parameter data[36] with the Union2.1 and BAO data to show effects of the Hubble parameter data. The results are shown in Table 6 and Fig. 3. With the addition of the 22 Hubble date points, FoM is improved, but not as much as that with shift parameter R. Though one needs not to have integration in fitting Hubble data, the errors of Hubble data is much bigger than that of shift parameter R date and the width of second bin related to the Hubble data is much smaller than that of R date.

z_1	w_1	w_2	FoM
0.4	$-1.01^{+0.06+0.11}_{-0.07-0.14}$	$-1.01^{+0.23+0.40}_{-0.32-0.77}$	50.93
0.5	$-1.01^{+0.06+0.12}_{-0.06-0.13}$	$-1.05^{+0.32+0.51}_{-0.57-1.40}$	30.89
0.6	$-1.02^{+0.06+0.11}_{-0.07-0.13}$	$-1.10^{+0.46+0.71}_{-0.94-4.67}$	9.12
0.7	$-1.02^{+0.05+0.10}_{-0.08-0.15}$	$-1.10^{+0.61+0.84}_{-1.70-16.84}$	4.96

Table 6 The best-fitted values and their 68.3% and 95.4% C.L. errors of w_1 and w_2 from data of SN+A+H, the divided positions are $z_1 = 0.4, 0.5, 0.6, 0.7$, respectively.

5 Summary

We have analyzed constraints of w_{de} at high redshift from current and future observations. It was shown that

at higher redshift, constraints of w_{de} from all observational data sets are much weaker. The present data give poor constraints on w_{de} beyond $z \sim 0.4$, whose average 95.4% C.L. error is 0.86. With the future 2298 mock data, average 95.4% C.L. error of w_{de} beyond $z \sim 0.4$ is about 0.43. We have carefully analyzed why constraints of DE at high redshift from observational data are so poor. Since almost all DE data is of distance type, our analyses are mainly based on distance type of data. The analyses show that it is hard to get good constraints of w_{de} at high redshift from distance type of data. Then we tried to improve constraints of DE at high redshift by adding more numbers of future mock SNIa data, improving the errors of observational data, and combining other type of data (Hubble parameter data) with distance types of data. It was shown that improving the error of observations is the most efficient way. About 6900 SNIa data with observational errors $\sigma = 0.02$ can constrain w_{de} beyond $z = 1$ within 0.1 at 68.3% C.L. and within 0.2 at 95.4% C.L. .

At present, many projects for DE are in progress or in planning. It is expected that a great deal of data points will be released. The distance types of data will still be the most important ones for revealing the nature of DE. To reveal the nature of DE, good constraints of w_{de} at high redshift is required. Our results show that much more data points will be needed, but improvements for accuracy of the observations are much more efficient and necessary. While the most present observational data for DE are distance type or can be converted into distance type, another way to improve the constraints of w_{de} is developing more other types of data.

Acknowledgements:

This work was supported in part by the National Natural Science Foundation of China (No. 11247008, No. 11175225 and No. 11147186), in part by Zhejiang Provincial Natural Science Foundation of China under Grant No. LQ12A05004, and in part by the Ministry of Science and Technology of China under Grant No. 2010CB833004 and No. 2010CB832805.

References

1. A. G. Riess *et al.* [Supernova Search Team Collaboration], *Astron. J.* **116** (1998) 1009 [astro-ph/9805201].
2. S. Perlmutter *et al.* [Supernova Cosmology Project Collaboration], *Astrophys. J.* **517** (1999) 565 [astro-ph/9812133].
3. P. J. E. Peebles and B. Ratra, *Rev. Mod. Phys.* **75** (2003) 559 [astro-ph/0207347].
4. E. J. Copeland, M. Sami and S. Tsujikawa, *Int. J. Mod. Phys. D* **15** (2006) 1753 [hep-th/0603057].
5. P. J. Steinhardt, L. -M. Wang and I. Zlatev, *Phys. Rev. D* **59** (1999) 123504 [astro-ph/9812313].
6. S. Capozziello, S. Carloni and A. Troisi, *Recent Res. Dev. Astron. Astrophys.* **1** (2003) 625 [astro-ph/0303041].
7. R. -G. Cai, *Phys. Lett. B* **657** (2007) 228 [arXiv:0707.4049 [hep-th]].
8. R. -G. Cai and Q. Su, *Phys. Rev. D* **81** (2010) 103514 [arXiv:0912.1943 [astro-ph.CO]].
9. R. -G. Cai, Z. -L. Tuo, H. -B. Zhang and Q. Su, *Phys. Rev. D* **84** (2011) 123501 [arXiv:1011.3212 [astro-ph.CO]].
10. M. Chevallier and D. Polarski, *Int. J. Mod. Phys. D* **10** (2001) 213 [gr-qc/0009008].
11. E. V. Linder, *Phys. Rev. Lett.* **90** (2003) 091301 [astro-ph/0208512].
12. A. R. Cooray and D. Huterer, *Astrophys. J.* **513** (1999) L95 [astro-ph/9901097].
13. D. Huterer and M. S. Turner, *Phys. Rev. D* **64** (2001) 123527 [astro-ph/0012510].
14. D. Huterer and G. Starkman, *Phys. Rev. Lett.* **90** (2003) 031301 [astro-ph/0207517].
15. D. Huterer and A. Cooray, *Phys. Rev. D* **71** (2005) 023506 [astro-ph/0404062].
16. Y. Wang, *Phys. Rev. D* **80** (2009) 123525 [arXiv:0910.2492 [astro-ph.CO]].
17. T. Holsclaw, U. Alam, B. Sanso, H. Lee, K. Heitmann, S. Habib and D. Higdon, *Phys. Rev. D* **82** (2010) 103502 [arXiv:1009.5443 [astro-ph.CO]].
18. S. Sullivan, A. Cooray and D. E. Holz, *JCAP* **0709** (2007) 004 [arXiv:0706.3730 [astro-ph]].
19. G. -B. Zhao, D. Huterer and X. Zhang, *Phys. Rev. D* **77** (2008) 121302 [arXiv:0712.2277 [astro-ph]].
20. P. Serra, A. Cooray, D. E. Holz, A. Melchiorri, S. Pandolfi and D. Sarkar, *Phys. Rev. D* **80** (2009) 121302 [arXiv:0908.3186 [astro-ph.CO]].
21. R. -G. Cai, Q. Su and H. -B. Zhang, *JCAP* **1004** (2010) 012 [arXiv:1001.2207 [astro-ph.CO]].
22. A. Hojjati, L. Pogossian and G. -B. Zhao, *JCAP* **1004** (2010) 007 [arXiv:0912.4843 [astro-ph.CO]].
23. Q. Su, X. He and R. -G. Cai, arXiv:1204.2146 [astro-ph.CO].
24. Y. Wang and S. Wang, *Phys. Rev. D* **88** (2013) 4, 043522 [arXiv:1304.4514 [astro-ph.CO]].
25. Y. Wang, *Phys. Rev. D* **77** (2008) 123525 [arXiv:0803.4295 [astro-ph]].
26. Q. Su, Z. -L. Tuo and R. -G. Cai, *Phys. Rev. D* **84** (2011) 103519 [arXiv:1109.2846 [astro-ph.CO]].
27. N. Suzuki, D. Rubin, C. Lidman, G. Aldering, R. Amanullah, K. Barbary, L. F. Barrientos and J. Botyanszki *et al.*, *Astrophys. J.* **746** (2012) 85 [arXiv:1105.3470 [astro-ph.CO]].
28. D. J. Eisenstein *et al.* [SDSS Collaboration], *Astrophys. J.* **633** (2005) 560 [astro-ph/0501171].
29. D. Stern, R. Jimenez, L. Verde, M. Kamionkowski and S. A. Stanford, *JCAP* **1002** (2010) 008 [arXiv:0907.3149 [astro-ph.CO]].
30. A. G. Kim, E. V. Linder, R. Miquel and N. Mostek, *Mon. Not. Roy. Astron. Soc.* **347** (2004) 909 [astro-ph/0304509].
31. A. Ealet *et al.* [SNAP Collaboration], [astro-ph/0210087].
32. I. Maor, R. Brustein and P. J. Steinhardt, *Phys. Rev. Lett.* **86** (2001) 6 [Erratum-ibid. **87** (2001) 049901] [astro-ph/0007297].
33. D. H. Weinberg, M. J. Mortonson, D. J. Eisenstein, C. Hirata, A. G. Riess and E. Rozo, *Phys. Rept.* **530** (2013) 87 [arXiv:1201.2434 [astro-ph.CO]].
34. G. Hinshaw *et al.* [WMAP Collaboration], *Astrophys. J. Suppl.* **208** (2013) 19 [arXiv:1212.5226 [astro-ph.CO]].

-
35. P. A. R. Ade *et al.* [Planck Collaboration], Astron. Astrophys. (2014) [arXiv:1303.5076 [astro-ph.CO]].
 36. O. Farooq, D. Mania and B. Ratra, arXiv:1308.0834 [astro-ph.CO].